Solute diffusion is hindered in the mitochondrial matrix

Cindy E. J. Dieteren[a,b], Stan C. A. M. Gielen[c], Leo G. J. Nijtmans[b], Jan A. M. Smeitink[b], Herman G. Swarts[a], Roland Brock[a], Peter H. G. M. Willems[a], and Werner J. H. Koopman[a,1]

[a]Department of Biochemistry, Nijmegen Centre for Molecular Life Sciences, Radboud University Nijmegen Medical Centre, P.O. Box 9101, NL-6500 HB, Nijmegen, The Netherlands; [b]Department of Pediatrics, Nijmegen Centre for Mitochondrial Disorders, Radboud University Nijmegen Medical Centre, P.O. Box 9101, NL-6500 HB, Nijmegen, The Netherlands; and [c]Department of Biophysics, Donders Institute for Brain, Cognition and Behaviour, Radboud University Nijmegen Medical Centre, P.O. Box 9101, NL-6500 HB, Nijmegen, The Netherlands

Edited by Roland Douce, Institut de Biologie Structurale, Grenoble Cedex 1, France, and approved April 12, 2011 (received for review November 24, 2010)

Intracellular chemical reactions generally constitute reaction-diffusion systems located inside nanostructured compartments like the cytosol, nucleus, endoplasmic reticulum, Golgi, and mitochondrion. Understanding the properties of such systems requires quantitative information about solute diffusion. Here we present a novel approach that allows determination of the solvent-dependent solute diffusion constant ($D_{solvent}$) inside cell compartments with an experimentally quantifiable nanostructure. In essence, our method consists of the matching of synthetic fluorescence recovery after photobleaching (FRAP) curves, generated by a mathematical model with a realistic nanostructure, and experimental FRAP data. As a proof of principle, we assessed $D_{solvent}$ of a monomeric fluorescent protein (AcGFP1) and its tandem fusion (AcGFP1^2) in the mitochondrial matrix of HEK293 cells. Our results demonstrate that diffusion of both proteins is substantially slowed by barriers in the mitochondrial matrix (cristae), suggesting that cells can control the dynamics of biochemical reactions in this compartment by modifying its nanostructure.

molecular dynamics | quantitative random-walk model | systems biology

A major challenge facing biochemistry is to understand the dynamics of chemical reactions within inhomogeneous cell compartments like the cytosol, nucleus, endoplasmic reticulum (ER), Golgi, and mitochondrion (1). In general, intracompartment reactions involve the conversion of (im)mobile substrates by (im)mobile enzymes into (im)mobile products and therefore constitute reaction-diffusion systems. Obviously, gaining insight into the behavior of such systems requires quantitative information about solute diffusion. The latter depends on solvent and solute properties, the dimensions and shape of the compartment, and the internal structure of the compartment (2–6).

A widely used strategy to investigate solute diffusion involves expressing a fluorescent tracer protein (FP) in the compartment of interest. Next, FP mobility is measured using FCS (fluorescence correlation spectroscopy) or FRAP (fluorescence recovery after photobleaching). This is then followed by curve fitting and/or mathematical modeling of the experimental data to obtain the diffusion constant of the FP (7–16). However, these analysis methods generally do not include realistic (i.e., experimentally determined) information concerning the spatial dimensions and nanostructure of the compartment. Moreover, the temporal scale of most FRAP models does not quantitatively match with that of FRAP experiments. Therefore it was already recognized some time ago (8–17) that the above approaches will only yield an "apparent" (biased) value for the diffusion constant (D_{app}) of a given FP, which represents an underestimation of the "real" (i.e., purely solvent-dependent) diffusion constant ($D_{solvent}$).

In this study we present a strategy to determine $D_{solvent}$ inside cell compartments with an experimentally accessible nanostructure. Our method consists of matching synthetic FRAP curves, generated by a realistic 3D mathematical model, with experimental FRAP data. As a proof of principle, we assessed $D_{solvent}$ for a monomeric GFP-derived protein (AcGFP1) and its tandem fusion (AcGFP1^2) in the mitochondrial matrix within living cells. We chose this organelle for the following reasons (18–23): (*i*) Many intramatrix reactions involve the conversion of mobile substrates by immobilized membrane-bound enzymes into mobile products and thereby constitute reaction-diffusion systems; (*ii*) mitochondrial length can be considerable (e.g., 50 μm in fibroblasts), making solute diffusion particularly relevant; and (*iii*) mitochondria possess an interesting nanostructure, in which folds (cristae) of the mitochondrial inner membrane (MIM) protrude into the mitochondrial matrix compartment, potentially hindering intramatrix solute diffusion.

Our hybrid *in silico* and experimental approach revealed that FP diffusion in the mitochondrial matrix is severely hindered by cristae. Therefore, we propose that regulated alterations in compartment nanostructure allow the cell to control solute diffusion inside cellular compartments. This implies that alterations in mitochondrial nanostructure, as observed during numerous (patho)physiological conditions, can affect the properties of intramatrix reaction-diffusion systems and thereby mitochondrial and cellular function.

Results

A Quantitative Mathematical Model of Protein Diffusion in the Mitochondrial Matrix. To allow extraction of the solvent-dependent diffusion constant ($D_{solvent}$) of a given FP from experimental FRAP curves, we developed a 3D diffusion model. This model was constrained by experimental data as follows: (*i*) the length (L_{mito}) and radius (R_{mito}) of the mitochondrion, (*ii*) the number (n) of diffusion barriers inside the mitochondrion, (*iii*) the FP concentration in the mitochondrial compartment (C_P), and (*iv*) the dimensions of the experimental FRAP region (S_{FRAP}). Our strategy was to match the kinetics of the simulated and experimental FRAP curve, as reflected by their FRAP recovery time constant (T_{FRAP}), by varying the value of $D_{solvent}$ in the model (Fig. 1*A*). Structurally, the mitochondrion is modeled as a closed cylinder with $R_{mito} = 0.27 \pm 0.035$ μm and $L_{mito} = 4.0 \pm 0.14$ μm ($N = 45$), which were determined experimentally for the HEK293 cells used in this study (13, 16). To account for possible hindrance of FP diffusion by the mitochondrial nanostructure, we performed electron microscopy (EM) analysis of mitochondria in HEK293 cells (e.g., Fig. 1*B*). This revealed that each mitochondrion on average contained between 6.2–8.2 cristae

Author contributions: P.H.G.M.W. and W.J.H.K. designed research; C.E.J.D. performed research; S.C.A.M.G., L.G.J.N., and H.G.S. contributed new reagents/analytic tools; C.E.J.D. and W.J.H.K. analyzed data; and J.A.M.S., R.B., P.H.G.M.W., and W.J.H.K. wrote the paper.

The authors declare no conflict of interest.

This article is a PNAS Direct Submission.

[1]To whom correspondence should be addressed. E-mail: w.koopman@ncmls.ru.nl.

This article contains supporting information online at www.pnas.org/lookup/suppl/doi:10.1073/pnas.1017581108/-/DCSupplemental.

BIOPHYSICS AND COMPUTATIONAL BIOLOGY

Downloaded at Palestinian Territory, occupied on December 23, 2021

www.manaraa.com

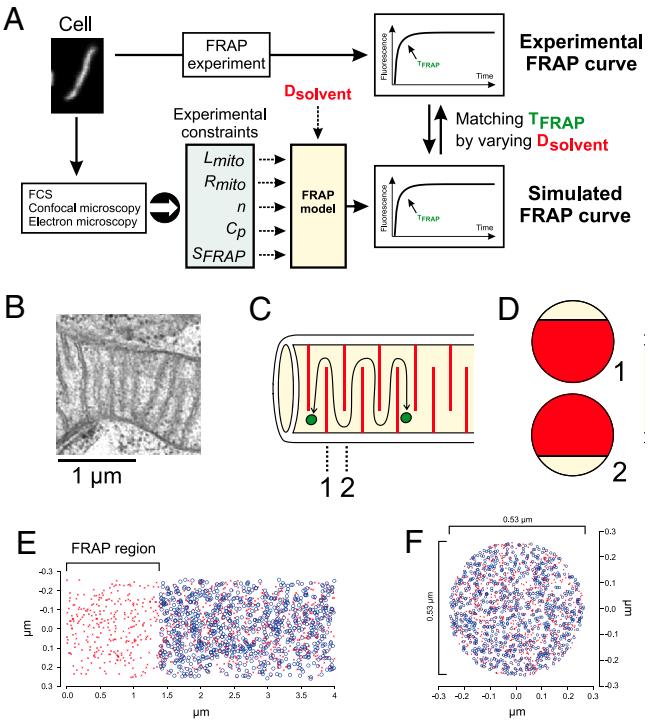

Fig. 1. Strategy to determine the diffusion properties of proteins inside a nanostructured cellular compartment. (*A*) Our method consists of experimentally determining the FRAP time constant (T_{FRAP}) of a fluorescent protein in the mitochondrial matrix and parallel generation of simulated FRAP curves by a quantitative model. Importantly, experimental constraints are imposed on the model. The solvent-dependent solute diffusion constant ($D_{solvent}$) can be predicted by matching the simulated T_{FRAP}-value with the experimental T_{FRAP}-value through varying $D_{solvent}$ in the model. (*B*) Typical electron microscopy image revealing cristae nanostructure in an AcGPF1-expressing HEK293 cell. (*C*) Internal geometry of the model; only part of the mitochondrion is shown. (*D*) Barrier geometry. (*E*) Simulated position of FP molecules directly following the bleach pulse at $t = 0$ s (blue circles) and 15 s later (red crosses) in a side view projection. (*F*) Similar to *E* but now for a top view projection.

per µm (95% confidence interval; $N = 26$ mitochondria), implying that a mitochondrion of length L_{mito} contains between 25–33 diffusion barriers. In the model, we accounted for the presence of cristae by including a number of n equidistant and partially overlapping barriers of negligible thickness with a semicircular shape (Fig. 1 *C* and *D*). We previously demonstrated using EYFP that intramatrix FP concentrations up to 10 µM do not affect FP diffusion (16). Therefore, in the model we assumed that individual FP molecules move independently and are present at a concentration of 10 µM. Because AcGFP1 is an inert monomeric FP (24), we further assumed that FP molecules were elastically reflected from the mitochondrial inner membrane (MIM). Before the start of each simulation, FP molecules were randomly positioned within the mitochondrial volume. Three-dimensional diffusion of FP molecules with a concentration of $C(x,y,z,t)$ at position (x, y, z) at time t is described by the equation:

$$\frac{\partial C(x,y,z,t)}{\partial t} = D_{\text{solvent}}\left\{\frac{\partial^2 C(x,y,z,t)}{\partial x^2} + \frac{\partial^2 C(x,y,z,t)}{\partial y^2} + \frac{\partial^2 C(x,y,z,t)}{\partial z^2}\right\}. \quad [1]$$

Importantly, $D_{solvent}$ represents the "real" solvent-dependent (barrier-independent) FP diffusion constant, which we want to extract from the FRAP experiments. Following FP bleaching at $t = 0$ s (i.e., the position of nonbleached FPs marked by blue circles in Fig. 1 *E* and *F*), the time course of FP redistribution during 15 simulated seconds was calculated (i.e., red crosses at $t = 15$ s in Fig. 1 *E* and *F*). Compatible with experiments (see below), nonbleached FPs fully redistributed across the mitochondrion during this time period. Simulated and experimental FRAP curves were analyzed in an identical way to allow comparison of their kinetic characteristics.

FRAP Analysis of Protein Mobility in the Mitochondrial Matrix of Living Cells. To determine FP mobility in the mitochondrial matrix we used inducible HEK293 cell lines (15). These expressed AcGFP1 or its tandem fusion AcGFP1[2] in the mitochondrial matrix (Fig. 2 *A* and *B*). A typical FRAP experiment is depicted in Fig. 2*C*. Following the bleach pulse in the FRAP region (square), the fluorescence signal in the mitochondrion equilibrated within 15 s. Calculation of the FP mobile fraction (F_m) revealed values close to one (AcGFP1, 1.02; AcGFP1[2], 0.99), demonstrating that both FPs were fully mobile. For AcGFP1, fluorescence recovered with an average time constant T_{FRAP} of 0.60 ± 0.015 s (Fig. 2*D*). To rule out interference of processes unrelated to solute diffusion, we investigated how the FRAP kinetics depended on the size of the FRAP region in AcGFP1-induced cells. When the size of the FRAP region was increased twofold, recovery was twofold slower and F_m was not affected (Fig. S1). This demonstrates that T_{FRAP} reflects authentic FP diffusion (25). For AcGFP1[2], fluorescence recovered significantly slower than for AcGFP1 (T_{FRAP} of 1.78 ± 0.038 s; Fig. 2*D*), indicating that the mobility of matrix-soluble FPs decreases with increasing MW.

Quantifying Protein Diffusion by Matching Simulated with Experimental FRAP Data. Increasing the number of barriers in the model led to a progressive reduction in the rate of fluorescence recovery (Fig. 3*A*). The effect of fixed barriers on FP diffusion can also be appreciated by quantifying the fluorescence loss in photobleaching (FLIP) in a region distal from the FRAP region (7). Therefore, we also simulated the FLIP signal in a region with size S_{FRAP}, located 1.2 µm away from the FRAP region (i.e., at the other tip of the mitochondrion; Fig. 3*A*, *Inset*). The rate of FLIP decreased when the number of barriers increased (Fig. 3*B*). Kinetic analysis further revealed a delay (dt) between the onset of fluorescence recovery in the FRAP region and onset of

Downloaded at Palestinian Territory, occupied on December 23, 2021
www.manaraa.com

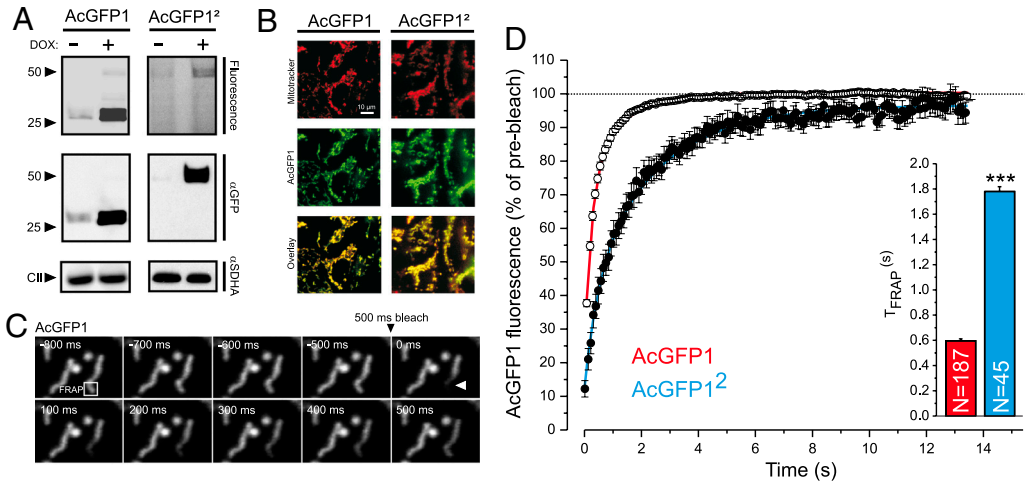

Fig. 2. FRAP analysis of mitochondrial AcGFP1 and AcGFP1^2 in HEK293 cells. (*A*) SDS/PAGE fluorogram (top panels) and anti-EGFP antibody immunodetection (middle panels) of mitochondrial matrix-targeted AcGFP1 and AcGFP1^2 in HEK293 cells in the absence (–) and presence (+) of the expression inducer doxycycline (DOX). The lower panels show the expression level of the CII loading control (detected using an anti-SDHA antibody). Closed arrowheads indicate MW (in kDa; upper panels) and CII (lower panel). (*B*) Confocal images showing mitochondrial colocalization of AcGFP1/AcGFP1^2 fluorescence and Mitotracker Red CM-H_2XROS following expression induction. (*C*) Typical example of images acquired during a FRAP experiment in cells expressing mitochondria-targeted AcGFP1. Following a 500-ms bleach pulse (triangle) in the FRAP region (square), AcGFP1 fluorescence rapidly redistributed across the mitochondrial filament. (*D*) Average fluorescence recovery curve and the fitted single-component exponential model (lines) for AcGFP1 and AcGFP1^2. R^2 values of the fit equaled: 0.98 (AcGFP1-induced) and 0.99 (AcGFP1^2-induced). The inset shows the time constant (T_{FRAP}) of the recovery curve for the two fluorescent proteins. In this figure, values on the Y-axis represent the average of the indicated number (N) of recorded mitochondria in at least three independent experiments. The error bars represents SE (average curves) or SEM (bar graphs). Statistics: significantly different from AcGFP1 (***$p < 0.001$).

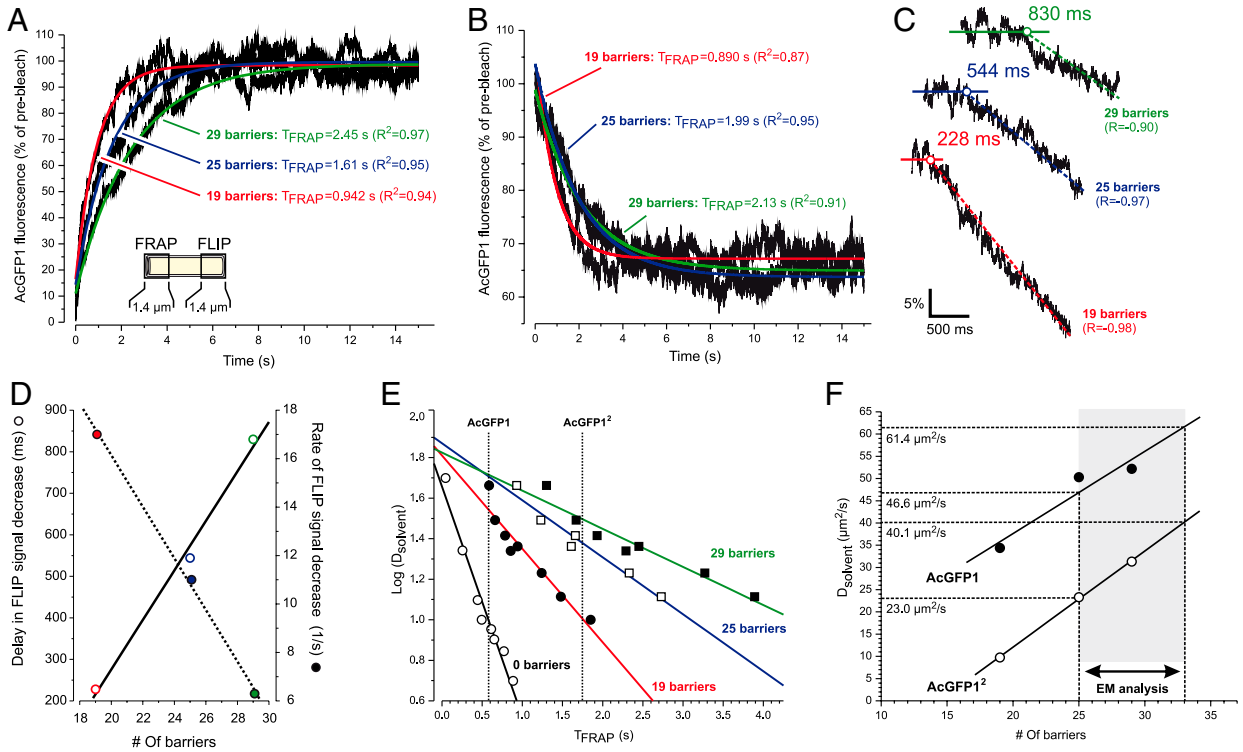

Fig. 3. Application of the mathematical model to predict diffusion constants. (*A*) Simulated FRAP curve for an FP with a $D_{solvent}$ of 23 $\mu m^2 \cdot s^{-1}$ in the presence of 19, 25, or 29 diffusion barriers. A single-component exponential model, yielding a time constant T_{FRAP}, adequately fitted the data. (*B*) Simulated fluorescence loss in photobleaching (FLIP) curve for a region at the other tip of the mitochondrion. T_{FRAP} was obtained as described for *A*. (*C*) Magnification of *B* (each curve starting at $t = 0$ s) revealing that the time-lag (*dt*) in the onset (open symbol) of FLIP increases, whereas the rate of FLIP becomes slower, upon increasing the number of barriers. (*D*) Linear relationship between the number of barriers and *dt* (open symbols) and the number of barriers and the absolute rate of fluorescence decrease in the FLIP region (filled symbols). (*E*) Effect of varying $D_{solvent}$ in the model on the recovery time of the simulated FRAP curve (T_{FRAP}) in the presence of 0, 19, 25, and 29 diffusion barriers. A linear relationship between $\log(D_{solvent})$ and T_{FRAP} was found. (*F*) Linear relationship between $D_{solvent}$ and the number of barriers. For both AcGFP1 and AcGFP1^2, three data points are given. These reflect the three values of $D_{solvent}$ predicted by the model for 19, 25, and 29 diffusion barriers using the T_{FRAP} determined experimentally. From the fitted lines, $D_{solvent}$ values were determined (dotted lines) using the number of diffusion barriers (cristae) determined by EM analysis. All linear fits in this figure had a *p*-value <0.05 and an *R*-value of 0.95–0.99 (positive correlations) or –0.96 (negative correlations).

Downloaded at Palestinian Territory, occupied on December 23, 2021

www.manaraa.com

fluorescence decrease in the FLIP region (Fig. 3*C*). The time delay and the rate of fluorescence decay in the FLIP region linearly increased and decreased, respectively, with the number of barriers (Fig. 3*D*). For 29 barriers *dt* equaled 830 ms, meaning that FPs travelled the distance between the FRAP and FLIP region at an average speed of 1.5 $\mu m \cdot s^{-1}$. The latter value is compatible with the "apparent" linear diffusion velocity of the FP mitoDsRed1 (1.0 $\mu m \cdot s^{-1}$) in HeLa cells (20) and the rapid FP exchange between fusing mitochondria (e.g., 26).

Next, we determined how varying $D_{solvent}$ affected T_{FRAP} in the presence of 0, 19, 25, and 29 diffusion barriers (Fig. 3*E*; different symbols). It was found that T_{FRAP} increased linearly with decreasing $\log(D_{solvent})$ for "unhindered" diffusion (0 barriers) and hindered diffusion (19, 25, and 29 barriers). This allows calculation of the experimental $D_{solvent}$ values by inserting the experimental T_{FRAP} values for AcGFP1 and AcGFP1^2 into the linear fitting equations used to describe the data (Fig. 3*E*; lines). In this way, four predicted values for $D_{solvent}$ were obtained (i.e., in case of 0, 19, 25, and 29 diffusion barriers) for both AcGFP1 and AcGFP1^2.

In case of 0 barriers, $D_{solvent}$-values equaled 9.54 $\mu m^2 \cdot s^{-1}$ and 0.427 $\mu m^2 \cdot s^{-1}$ for AcGFP1 and AcGFP1^2, respectively. Subsequently, we used the three remaining $D_{solvent}$-values (19, 25, and 29 barriers) for AcGFP1 and AcGFP1^2 to establish the relationship between the number of diffusion barriers and $D_{solvent}$. This yielded two linear relationships (Fig. 3*F*). Finally, we combined information about the number of barriers determined by EM analysis (shaded area) with the fitted lines. This predicted (dotted lines) that AcGFP1 and AcGFP1^2 have a $D_{solvent}$ between 46.6–61.4 $\mu m^2/s$ and 23.0–40.1 $\mu m^2/s$, respectively. This means (see *Materials and Methods*) that the solvent-dependent viscosity of the mitochondrial matrix ($\eta_{solvent}$) is between 1.50–1.97 cP (i.e., 1.5-fold to twofold higher than pure water).

Discussion

In living cells, understanding the properties of compartmentalized reactions requires quantitative information about intracompartment solute diffusion. Here a strategy is presented allowing determination of the solvent-dependent diffusion constant ($D_{solvent}$) inside cell compartments with an experimentally quantifiable nanostructure. To demonstrate the feasibility of this approach we determined $D_{solvent}$ for an inert monomeric FP (AcGFP1) and its tandem fusion (AcGFP1^2) inside the mitochondrial matrix. To this end we constructed a realistic mathematical FRAP model and quantified $D_{solvent}$ by matching the kinetics of the simulated and experimental FRAP curves.

A combination of FRAP and mathematical modeling was used previously to investigate FP diffusion inside the ER, but these studies did not consider the internal nanostructure of this compartment (27, 28). In the case of mitochondria, we are aware of only two other reports that applied mathematical modeling to analyze submitochondrial FRAP experiments (7, 8). Our strategy differs from these studies as follows: (*i*) It is constrained by experimental values for the dimensions of the compartment, its internal nanostructure, intracompartment FP concentration, and the size of the FRAP region; (*ii*) it has a temporal and fluorescence intensity scale that quantitatively match those of experiments without the need for rescaling; (*iii*) it can be used with data obtained from "classical" FRAP experiments instead of "fast" spot-FRAP techniques, which requires specialized equipment; and (*iv*) it applies a unique computational approach to account for intracompartment diffusion hindrance (see below).

Our model predicts how intramatrix diffusion barriers affect free FP diffusion. External and internal model geometry was based on experimental data in HEK293 cells concerning mitochondrial length, diameter, and size of the FRAP region. These parameters, as well as matrix GFP concentration (C_p), were determined by confocal microscopy and FCS and have a fixed value in the model. Therefore the value of $D_{solvent}$ predicted by the model only depends on the number of diffusion barriers. To compute the synthetic FRAP curves, the model takes into account the increased distance that the FP has to diffuse when it moves around the barriers. This means that the exact topology of the barriers is not of major importance. Therefore our EM analysis can be considered as an estimate of mitochondrial cristae shape and number.

For the 0-barrier model the obtained $D_{solvent}$-values predict (Eq. **6**) that the mitochondrial matrix is 10 times more viscous than pure water (i.e., $\eta_{solvent} = 9.7$ cP). A key determinant of matrix solvent viscosity is the concentration of macromolecules. In case of human serum albumin (HSA), an aqueous solution at 20 °C with a viscosity of 9.7 cP contains 313 mg/mL of protein (29). Analysis of mitochondrial homogenates revealed a protein concentration up to 500 mg/mL (e.g., 30), compatible with our 0-barrier model. However, in reality mitochondria contain cristae. Moreover, the obtained $D_{solvent}$-values for the 0-barrier model are far below the D_{app} values reported in FRAP and FCS experiments, which already account for effects of diffusion hindrance (e.g., 8, 13). This demonstrates that a 0-barrier model is inappropriate for describing intramatrix FP diffusion.

Our "hindered" models predict a fivefold lower viscosity of the mitochondrial matrix solvent, equivalent with a HSA concentration of 130 mg/mL (29). This means that a substantial part of the mitochondrial proteins are not present as solutes in the mitochondrial matrix. The latter is compatible with the fact that four of the most abundant mitochondrial proteins (ATP5A1, ATP5B, ANT1, and ANT2) are membrane-bound (31). Similarly, key enzymes of the matrix-residing tricarboxylic acid (TCA) cycle are immobilized (32). Also the multiprotein complexes of the mitochondrial oxidative phosphorylation (OXPHOS) system are membrane-bound (23). Taken together, our results predict that (*i*) the mitochondrial matrix possesses a moderate viscosity (i.e., approximately twofold higher than pure water) and (*ii*) intramatrix FP diffusion is substantially hindered by diffusion barriers (cristae). These findings argue against the presence of a central mitochondrial "water channel" allowing rapid unhindered FP diffusion (8, 17).

We assumed during our simulations that the 500-ms bleaching pulse in the FRAP region does not alter mitochondrial ultrastructure. This assumption was based on the following data: (*i*) Intense AcGFP1 illumination is not phototoxic (24); (*ii*) photobleaching does not alter the morphology of cell surface membranes (33) nor the lateral mobility of plasma membrane proteins (34); (*iii*) targeted photodamage of mitochondria induces their fragmentation (35), which was not observed in our experiments; and (*iv*) we did not detect alterations in mitochondrial diameter within the FRAP region. In a worst-case scenario the cristae within the FRAP region would be completely destroyed, reducing the number of diffusion barriers in the model. However, this would not affect the main conclusion of our study, namely that matrix diffusion barriers are essential to quantitatively explain our FRAP results.

The obtained AcGFP1 diffusion constant is approximately twofold lower than in pure water. Importantly, this is the "real" diffusion constant ($D_{solvent}$) and not the "apparent" diffusion constant. The value obtained for $D_{solvent}$ is not directly informative about the absolute speed with which a solute diffuses in the matrix, because it does not account for the effect of diffusion hindrance. This concept is illustrated by our calculation of the (hindered) linear GFP diffusion velocity (Fig. 3*C*), which is in agreement with previous studies (20, 26).

Our results demonstrate that FP diffusion in the mitochondrial compartment decreases with the MW of the protein and, in sharp contrast to the current biological dogma (17), is severely hindered by the presence of diffusion barriers. These findings are important because changes in mitochondrial ultrastructure, viscosity, and metabolic state often occur in parallel (13, 21, 22, 36, 37).

Downloaded at Palestinian Territory, occupied on December 23, 2021
www.manaraa.com

For instance, matrix solute diffusion differs significantly between different mitochondrial respiratory states (38). Moreover, matrix volume changes causing alterations in the concentration of enzymes, their substrates, and metabolites probably play a role in metabolic control (30). Furthermore, we provided evidence that assembly of an important OXPHOS complex (complex I), involves intramatrix diffusion of subassemblies (15). This suggests that the diffusion properties of the matrix solvent are important during the complex I assembly reaction. In this sense, our findings suggest that changes in compartment nanostructure can greatly affect solute diffusion and thereby the dynamics of diffusion-limited reactions. Similarly, in *Dictyostelium* reorganization of the cytosolic acting meshwork has been linked to alterations in protein mobility (39). In principle, our approach is applicable to cellular compartments of which the 3D nanostructure can be experimentally accessed, for instance by EM analysis. For such compartments, cell-controlled changes in their internal nanostructure might also function to regulate intracompartment reaction dynamics.

Materials and Methods

Generation of Inducible Cell Lines. Stably transfected human embryonic kidney (HEK293) cell lines conditionally expressing AcGFP1 or its tandem fusion (AcGFP1^2) in the mitochondrial matrix were generated and cultured as described previously (15, 40). AcGFP1 and AcGFP1^2 expression was induced by adding 1 μg/mL doxycycline (DOX; Sigma) to the culture medium, followed by 24 h incubation.

SDS/PAGE and BN-PAGE analysis. Native mitochondrial proteins were isolated and run on SDS/PAGE gels as described before (15, 40). Following electrophoresis, Western blotting was performed as described previously (15, 40).

Colocalization Analysis. Colocalization analysis of AcGFP1 fluorescence and a mitochondrial marker dye (Mitotracker Red CM-H_2XROS; Invitrogen) was performed using confocal microscopy as described previously (41).

FRAP Experiments. Fluorescence recovery after photobleaching (FRAP) experiments were performed as described previously (15) using a ZEISS LSM510 Meta confocal microscope (Carl Zeiss). FRAP measurements were carried out at 20 °C to minimize mitochondrial movement (42). Images were acquired at a rate of 10 Hz using a 63x oil immersion objective (N.A. 1.4; Carl Zeiss), a zoom factor of 4 and an optical section thickness of <2 μm. Only single nonmoving mitochondria of constant length and diameter that were fully within the focal plane were analyzed. A FRAP region of 1.4 μm × 1.4 μm was used and FP photobleaching was performed during 500 ms using 488-nm light. Only mitochondria in which FRAP was paralleled by FLIP in a part distal to the FRAP region were considered to possess a continuous mitochondrial matrix and included in the analysis. FRAP was monitored using a HFT488 beam splitter and a LP505 emission filter. Individual FRAP curves (F(t)) were calculated as described previously (11):

$$F(t) = 100 \times \frac{(F(t)_{\text{FRAP region}} - F(t)_{\text{background}})}{(F(t)_{\text{total mito}} - F(t)_{\text{background}})} \times \frac{(F_{i,\text{total mito}} - F_{\text{background}})}{(F_{i,\text{FRAP region}} - F_{\text{background}})}. \quad [2]$$

Here the fluorescence intensity in the bleached mitochondrial region ($F(t)_{\text{FRAP region}}$) and for the total mitochondrion ($F(t)_{\text{total mito}}$) is background-corrected ($F(t)_{\text{background}}$) at each time point. Next, the corrected fluorescence signal in the bleached region is divided by the corrected intensity of the total mitochondrion to correct for the loss of fluorescence during the bleach. The data are normalized to the background-corrected prebleach intensity ($F_{i,\text{total mito}}$ and $F_{i,\text{FRAP region}}$) and multiplied by 100 to yield a percentage of prebleach fluorescence. Mean recovery curves were fitted by a single-component exponential model:

$$F(t) = y_0 + A \cdot (1 - e^{-t/T_{\text{FRAP}}}). \quad [3]$$

The mobile fraction (F_m) was calculated from mean recovery curves according to the equation (11, 12, 15, 43):

$$F_m = \frac{F_\infty - F_0}{F_{\text{initial}} - F_0}. \quad [4]$$

With F_∞ being the fluorescence intensity at $t = t_\infty$ (t_∞ was calculated from the fit in Eq. **3**: $F_\infty = y_0 + A$), F_0 being the starting fluorescence level of fluorescence recovery and F_{initial} being 100%.

Electron Microscopy (EM) Analysis. EM analysis was performed as described previously (14).

Image and Data Analysis. Image processing and analysis were performed using Image Pro Plus 6.3 (Media Cybernetics). Nonlinear curve fitting and statistical analysis was performed using Origin Pro 7.5 (Originlabs). Values from multiple experiments are expressed as mean ± SEM (standard error of the mean). Statistical significance (Bonferroni-corrected) was assessed using Student's *t*-test.

Numerical Simulations. Mathematical modeling was performed with MATLAB 6.1 (The Mathworks Inc.) using custom scripts. Diffusion described by Eq. **1** was simulated by adding a random displacement (Δx, Δy, Δz) at every time step ($\Delta t = 1$ ms), with Δx, Δy and Δz drawn from a normal distribution with zero mean and standard deviation: $\frac{1}{3}\sqrt{3}\sqrt{2D_{\text{solvent}}\Delta t}$. A normalization factor of $\frac{1}{3}\sqrt{3}$ for diffusion along each of the three dimensions *x*, *y*, and *z* was used to ensure that the 3D diffusion is equal to D_{solvent}. In the model the distance between neighboring barriers (ΔL_c) is given by: $\Delta L_c = L_{\text{mito}}/(n+1)$ and the matrix-protruding length of each barrier equals $2R_{\text{mito}} - \Delta L_c$. The distance between both sides of the cylinder (*v*) is given by $n+1$ times the length ($v = 2R_{\text{mito}} - \Delta L_c$) plus *n* times the distance (*w*) between two barriers on the same side of the cylinder ($w = \Delta L_c$). Therefore, a cylindrically shaped mitochondrion with length L_{mito} and radius R_{mito} containing *n* barriers can be approximated by a new cylinder of length $L_{\text{mito,new}}$:

$$L_{\text{mito,new}} = (n+1)\left(2R_{\text{mito}} - \frac{L_{\text{mito}}}{n+1}\right) + n\frac{L_{\text{mito}}}{n+1} = 2(n+1)R_{\text{mito}} - \frac{L_{\text{mito}}}{n+1}. \quad [5]$$

This means that increasing the number of diffusion barriers is equivalent to a longer cylinder with a smaller radius $R_{\text{mito,new}} = \frac{L_{\text{mito}}}{2(n+1)}$. This approximation is valid if *w* is smaller than $2R_{\text{mito}}$ (i.e., when the number of cristae is sufficiently large). Considering the experimental values for R_{mito} and L_{mito}, this implies that the number of barriers in the model should be 9 or larger. By adding barriers (i.e., by increasing the value of *n*) the FRAP region has a length of $L_{\text{mito}}/L_{\text{mito,new}}$ in the new equivalent cylinder. Because this equivalent cylinder is always longer in the presence (hindered model) than in the absence (unhindered model) of barriers, molecules have to diffuse over a longer distance before entering the FRAP region. Intuitively, this longer diffusion distance will result in a slower FRAP recovery and thereby a larger recovery time constant (T_{FRAP}) in the presence of barriers. The topological equivalence of a mitochondrial cylinder with diffusion barriers to a longer and thinner cylinder is a special case applying to mitochondria. This means that the previously described analytical solution for FP diffusion in a mitochondrial cylinder (7, 8) could also be used to iteratively determine D_{solvent}.

Calculation of Solvent Viscosity from the Protein Diffusion Constant. A modified version of the Stokes–Einstein relationship can be used to predict the solvent viscosity η_{solvent} (in centipoise; cP) for freely diffusing spherical and cylindrical FPs in an aqueous solution (44):

$$D_{\text{solvent}} = \frac{6.85 \cdot 10^{-8}\ \text{T}}{\eta_{\text{solvent}} \cdot \sqrt{M^{1/3} \cdot R_G}}. \quad [6]$$

Here, D_{solvent} represents the solvent-dependent FP diffusion constant (in $\text{cm}^2 \cdot \text{s}^{-1}$), *M* represents the FP molecular weight (MW; in $\text{g} \cdot \text{mol}^{-1}$), R_G represents the FP radius of gyration (in Å) and T indicates the temperature *T* (in K). For AcGFP1, *M* equals 29149 $\text{g} \cdot \text{mol}^{-1}$ and the R_G value can be calculated from the hydrodynamic radius (R_H) according to (45):

$$R_G = \sqrt{\frac{3}{5}} \cdot R_H. \quad [7]$$

For GFP, an R_H-value of 20 Å was reported (46), meaning that the R_G value of AcGFP1 equals 15.5 Å, compatible with molecular modeling results (45).

Downloaded at Palestinian Territory, occupied on December 23, 2021

www.manaraa.com

ACKNOWLEDGMENTS. We are grateful to Dr. J. Fransen and Ing. M. Wijers (Department of Cell Biology, Nijmegen Centre for Molecular Life Sciences, Radboud University Nijmegen Medical Centre) for electron microscopy analysis. This work was supported by grants of the Nederlandse organisatie voor Wetenschappelijk Onderzoek (NWO, Netherlands Organisation for Scientific Research, 911-02-008), the Radboud University Nijmegen Medical Centre, and the NWO Centres for Systems Biology Research initiative (CSBR09/013V).

1. Grima R, Schnell S (2006) How reaction kinetics with time-dependent rate coefficients differs from generalized mass action. *Chemphyschem* 7:1422–1424.
2. Jacob M, Schindler T, Balbach J, Schmid FX (1997) Diffusion control in an elementary protein folding reaction. *Proc Natl Acad Sci USA* 94:5622–5627.
3. Schnell S, Turner TE (2004) Reaction kinetics in intracellular environments with macromolecular crowding simulations and rate laws. *Prog Biophys Mol Biol* 85:235–260.
4. Dix JA, Verkman AS (2008) Crowding effects on diffusion in solutions and cells. *Annu Rev Biophys* 37:247–263.
5. Lizana L, Bauer B, Orwar O (2008) Controlling the rates of biochemical reactions and signaling networks by shape and volume changes. *Proc Natl Acad Sci USA* 105:4099–4104.
6. Bénichou O, Chevalier C, Klafter J, Meyer B, Voituriez R (2010) Geometry-controlled kinetics. *Nat Chem* 2:472–477.
7. Ölveczky BP, Verkman AS (1998) Monte Carlo analysis of obstructed diffusion in three dimensions: Application to molecular diffusion in organelles. *Biophys J* 74:2722–2730.
8. Partikian A, Ölveczky BP, Swaminathan R, Li Y, Verkman AS (1998) Rapid diffusion of green fluorescent protein in the mitochondrial matrix. *J Cell Biol* 140:821–829.
9. Lippincott-Schwartz J, Snapp E, Kenworthy A (2001) Studying protein dynamics in living cells. *Nat Rev Mol Cell Biol* 2:444–456.
10. Kim SA, Schwille P (2003) Intracellular applications of fluorescence correlation spectroscopy: Prospects for neuroscience. *Curr Opin Neurobiol* 13:583–590.
11. Goodwin JS, Kenworthy AK (2005) Photobleaching approaches to investigate diffusional mobility and trafficking of Ras in living cells. *Methods* 37:154–164.
12. Picard D, Suslova E, Briand PA (2006) 2-color photobleaching experiments reveal distinct intracellular dynamics of two components of the Hsp90 complex. *Exp Cell Res* 312:3949–3958.
13. Koopman WJH, et al. (2007) Partial complex I inhibition decreases mitochondrial motility and increases matrix protein diffusion as revealed by fluorescence correlation spectroscopy. *Biochim Biophys Acta Bioenergetics* 1767:940–947.
14. Koopman WJH, et al. (2008) Inherited complex I deficiency is associated with faster protein diffusion in the matrix of moving mitochondria. *Am J Physiol Cell Physiol* 294:C1124–C1132.
15. Dieteren CEJ, et al. (2008) Subunits of mitochondrial complex I exist as part of matrix- and membrane-associated subcomplexes in living cells. *J Biol Chem* 283:34753–34761.
16. Willems PHGM, Swarts HG, Hink MA, Koopman WJH (2009) The use of fluorescence correlation spectroscopy to probe mitochondrial mobility and intra-matrix protein diffusion. *Methods Enzymol* 456:287–302.
17. Verkman AS (2002) Solute and macromolecule diffusion in cellular aqueous compartments. *Trends Biochem Sci* 27:27–33.
18. Amchenkova AA, Bakeeva LE, Chentsov YS, Skulachev VP, Zorov DB (1988) Coupling membranes as energy-transmitting cables. I. Filamentous mitochondria in fibroblasts and mitochondrial clusters in cardiomyocytes. *J Cell Biol* 107:481–495.
19. Skulachev VP (2001) Mitochondrial filaments and clusters as intracellular power-transmitting cables. *Trends Biochem Sci* 26:23–29.
20. Collins TJ, Bootman MD (2003) Mitochondria are morphologically heterogeneous within cells. *J Exp Biol* 206:1993–2000.
21. Benard G, Rossignol R (2008) Ultrastructure of the mitochondrion and its bearing on function and bioenergetics. *Antioxid Redox Signal* 10:1313–1342.
22. Arismendi-Morillo G (2009) Electron microscopy morphology of the mitochondrial network in human cancer. *Int J Biochem Cell Biol* 41:2062–2068.
23. Koopman WJH, et al. (2010) Mammalian mitochondrial complex I: Biogenesis, regulation and reactive oxygen species generation. *Antioxid Redox Signal* 12:1431–1470.
24. Bulina ME, et al. (2006) A genetically encoded photosensitizer. *Nat Biotechnol* 24:95–99.
25. Periasamy N, Verkman AS (1998) Analysis of fluorophore diffusion by continuous distributions of diffusion coefficients: Application to photobleaching measurements of multicomponent and anomalous diffusion. *Biophys J* 75:557–567.
26. Twig G, et al. (2008) Fission and selective fusion govern mitochondrial segregation and elimination by autophagy. *EMBO J* 27:433–446.
27. Dayel MJ, Hom EFY, Verkman AS (1999) Diffusion of green fluorescent protein in the aqueous-phase lumen of endoplasmatic reticulum. *Biophys J* 76:2843–2851.
28. Sbalzarini I, Mezzacasa A, Helenius A, Koumoutsakos P (2005) Effects of organelle shape on fluorescence recovery after photobleaching. *Biophys J* 89:1482–1492.
29. Wetzel R, et al. (1980) Temperature behaviour of human serum albumin. *Eur J Biochem* 104:469–478.
30. Srere PA (1980) The infrastructure of the mitochondrial matrix. *Trends Biochem Sci* 5:120–121.
31. Calvo SE, Mootha VK (2010) The mitochondrial proteome and human disease. *Annu Rev Genomics Hum Genet* 11:25–44.
32. Haggie PM, Verkman AS (2002) Diffusion of tricarboxylic acid cycle enzymes in the mitochondrial matrix in vivo. Evidence for restricted mobility of a multienzyme complex. *J Biol Chem* 277:40782–40788.
33. Jacobson K, Hou Y, Wojcieszyn J (1978) Evidence for lack of damage during photobleaching measurements of the lateral mobility of cell surface components. *Exp Cell Res* 116:179–189.
34. Koppel DE, Sheetz MP (1981) Fluorescence photobleaching does not alter the lateral mobility of erythrocyte membrane glycoproteins. *Nature* 293:159–161.
35. Mai S, Klinkenberg M, Auburger G, Bereiter-Hahn J, Jendrach M (2010) Decreased expression of Drp1 and Fis1 mediates mitochondrial elongation in senescent cells and enhances resistance to oxidative stress through PINK1. *J Cell Sci* 123:917–926.
36. Mannella CA (2008) Structural diversity of mitochondria: functional implications. *Ann NY Acad Sci* 1147:171–179.
37. Sukhorukov VM, Bereiter-Hahn J (2009) Anomalous diffusion induced by cristae geometry in the inner mitochondrial membrane. *PLoS ONE* 4:e4604.
38. Scalettar BE, Abney JR, Hackenbrock CR (1991) Dynamics, structure and function are coupled in the mitochondrial matrix. *Proc Natl Acad Sci USA* 88:8057–8061.
39. Potma EO, et al. (2001) Reduced protein diffusion rate by cytoskeleton in vegetative and polarized dictyostelium cells. *Biophys J* 81:2010–2019.
40. Dieteren CEJ, Koopman WJH, Nijtmans LGJ (2009) Tracing human mitochondrial complex I assembly by use of GFP-tagged subunits. *Methods Enzymol* 456:133–151.
41. Vogel RO, et al. (2007) Cytosolic signaling protein Ecsit also localizes to mitochondria where it interacts with chaperone NDUFAF1 and functions in complex I assembly. *Genes Dev* 21:615–624.
42. Koopman WJH, Visch HJ, Smeitink JAM, Willems PHGM (2006) Simultaneous, quantitative measurement and automated analysis of mitochondrial morphology, mass, potential and motility in living human skin fibroblasts. *Cytometry A* 69A:1–12.
43. Chen Y, Lagerholm BC, Yang B, Jacobson K (2006) Methods to measure the lateral diffusion of membrane lipids and proteins. *Methods* 39:147–153.
44. He L, Niemeyer B (2003) A novel correlation for protein diffusion coefficients based on molecular weight and radius of gyration. *Biotechnol Prog* 19:544–548.
45. Dashevskaya S, Kopito RB, Friedman R, Elbaum M, Epel BL (2008) Diffusion of anionic and neutral GFP derivatives through plasmodesmata in epidermal cells of *Nicotiana benthamiana*. *Protoplasma* 234:13–23.
46. Terry BR, Matthews EK, Haseloff J (1995) Molecular characterisation of recombinant green fluorescent protein by fluorescence correlation microscopy. *Biochem Biophys Res Commun* 217:21–27.

Downloaded at Palestinian Territory, occupied on December 23, 2021

www.manaraa.com